Cross sections for $^3H(^7Li,n_0)^9Be$ and $^3H(^7Li,n_{tot})$

C. R. Brune, R. W. Kavanagh, S. E. Kellogg, and T. R. Wang
W. K. Kellogg Radiation Laboratory, California Institute of Technology, Pasadena, California 91125
(Received 5 September 1990)

The $^3H(^7Li,n_0)^9Be$ cross section was measured for $0.15 < E_{c.m.} < 1.24$ MeV at $\theta_{lab}=0°$, 45°, 90°, and 135° using Si(Li) diodes as neutron spectrometers. The $^3H(^7Li,n_{tot})$ cross section was measured for $0.05 < E_{c.m.} < 1.5$ MeV using a 4π neutron detector. The cross section for $^3H(^7Li,n_0)^9Be$ was used to calculate the thermonuclear reaction rate for the temperature range 0.3–10 GK. The results support predictions that ^9Be may be produced in quantities near spectroscopic limits of observation according to some models of inhomogeneous primordial nucleosynthesis.

I. INTRODUCTION

Current research in primordial nucleosynthesis has focused on the elemental abundances resulting from assuming an initially inhomogeneous baryon density. Such inhomogeneity is predicted to result from the quark-hadron phase transition in the early Universe, but the spatial distribution and magnitude of the inhomogeneity is largely uncertain.[1,2] Boyd and Kajino[3] first suggested that ^9Be may be produced in significant (observable) quantities in the inhomogeneous models of primordial nucleosynthesis via $^7Li(^3H,n_0)^9Be$. At the time of Boyd and Kajino's publication, the observational upper limits on ^9Be abundance in metal-deficient dwarfs[4] were above the level predicted, but recent observations[5] set an upper limit of

$$n(^9Be)/n(H) < 6.3\times10^{-14}$$

on ^9Be number abundance, within the range allowed for the nonuniform density model given in Kajino and Boyd's later publication.[6] The possibility of using the ^9Be abundance to constrain the parameters of the quark-hadron transition was pointed out by Malaney and Fowler.[7] However, a recent study by Terasawa and Sato[8] concludes that previous calculations of the ^9Be abundance overestimated the abundance by 2 orders of magnitude because previous authors used an oversimplified model of neutron diffusion.

All of the studies cited above have relied on estimates for the $^7Li(^3H,n_0)^9Be$ reaction rate, as the cross section had not been previously measured over the relevant energy range. Clearly, an experimental determination of the cross section is needed to improve the precision of the ^9Be abundance predicted by the various models. The cross section for $^7Li(^3H,n_{tot})$, which includes all neutron final states, has been studied previously,[9–12] but is not directly applicable to ^9Be production since all excited states of ^9Be are unstable against disintegration to ^8Be+n and other channels.

II. EXPERIMENTAL METHOD

The 3-MV Pelletron Tandem Accelerator at the Kellogg Radiation Laboratory was used to provide ^7Li beams, with $^7Li^-$ ions injected from a Cs sputter source. The accelerator-beam energy and the charge state were defined by a 90° analyzing magnet; the magnetic field was measured with an NMR gaussmeter. Energy calibration for α^+ particles was provided by the 0.606- and 1.530-MeV resonances[13,14] in $^{11}B(\alpha,n)$ and $^{24}Mg(\alpha,\gamma)$, respectively, and the same calibration ($\pm0.1\%$) was presumed to hold for $^7Li^+$ and $^7Li^{++}$. Beam-line and target vacuum were maintained less than 7×10^{-7} torr. At this pressure, we calculate that the fraction of the ^7Li beam undergoing charge exchange (and thus adding a systematic error to beam-current integration), in the length of the beam line between the last steering element and the target, to be at most 0.006 (estimated from the charge-exchange cross sections of Allison *et al.*[15] for lithium ions in nitrogen).

A. $^3H(^7Li,n_0)^9Be$

For the measurement of the $^3H(^7Li,n_0)^9Be$ cross section, a titanium-tritide (Ti-T) target on copper backing supplied by Amersham Corporation was used. The tritium areal density was determined by $^3H(p,n)^3He$ as described below (Sec. II B). Target uniformity and stability over time were also monitored with $^3H(p,n)^3He$ and found to be constant within 5%. To minimize target deterioration, the back of the target was cooled directly with flowing Freon. The beam spot was defined by a 3-mm Ta collimator 60 cm upstream from the target. To suppress secondary electrons, -400 V was placed on an insulated section of beam pipe ~10 cm downstream from the collimator. Beam current on target was maximized, and varied between 0.15 and 0.5 particle μA. Target current was integrated by an Ortec model 439 current integrator. Leakage current through the Freon cooling lines was measured, and found to be negligible (~0.3 nA).

Neutrons were detected with four room-temperature Si(Li) semiconductor detectors located outside the vacuum system at angles of $\theta_{lab}=0°$, 45°, 90°, and 135°. The detectors were supplied by EG&G Ortec and were nominally 5 mm deep. Three of the detectors had an active area of 75 mm^2, and the fourth had an active area of 200 mm^2. The target-detector distance varied from 1.8 to 6.5 cm. Most of the runs were taken with the detector faces

perpendicular to the incident neutrons. In the rest of the runs, the 200-mm^2 detector was oriented edge on to the incident neutrons in the 90° position to minimize the kinematic-energy spread of neutrons striking its large area, while the smaller detectors remained oriented for normal incidence.

Various aspects of the use of silicon semiconductor detectors as neutron spectrometers have been described previously.[16,17] Briefly, fast neutrons are detected by Si(Li) detectors through nuclear reactions that produce charged particles in the active volume of the detector. The neutrons interact primarily with ^{28}Si, which makes up 92.2% of natural silicon,[18] through the ^{28}Si$(n,\alpha)^{25}$Mg and ^{28}Si$(n,p)^{28}$Al reactions. The energy deposited in the detector is then the energy of the initiating neutron plus the Q value of the reaction. A spectrum produced by one of our detectors under bombardment by monoenergetic neutrons is shown in Fig. 1. In our experiment, the events due to ^{28}Si$(n,\alpha_0)^{25}$Mg ($Q=-2654$ keV) were used to measure cross sections. The ^{28}Si$(n,\alpha_0)^{25}$Mg cross section as measured twice previously[16,17] is shown in Figs. 2 and 3; although there is fair agreement in the region of overlap (Fig. 3), the evident discrepancies lead us to assign a ±15% error to our detection efficiencies. The efficiency for detecting neutrons by this method is rather low: roughly 0.03% of 15-MeV neutrons passing through 5 mm of Si react via ^{28}Si$(n,\alpha_0)^{25}$Mg.[16] The neutrons from ^{3}H(^{7}Li,n_0)^{9}Be measured in our experiment varied in energy from 8.0 to 14.3 MeV, which is in the range of energies previously studied.[16] Fortunately, of all of the possible neutron-producing reactions involving ^{3}H+^{7}Li, ^{3}H(^{7}Li,n_0)^{9}Be produces the neutron with the highest energy, so the peak of interest is not obscured by other reaction channels. The peaks in the Si(Li) detector spectrum due to ^{28}Si$(n,\alpha_0)^{25}$Mg and ^{28}Si$(n,\alpha_1)^{25}$Mg are separated by 585 keV, so the kinematic spread of the neutrons incident on the detector must be kept well below this level to maintain adequate resolution.

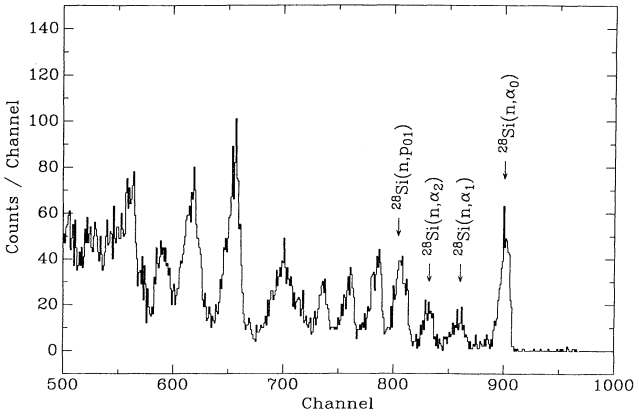

FiG. 1. Si(Li) pulse-height spectrum produced by 15.34-MeV neutrons from ^{3}H(d,n) at $\theta_{lab}=0°$ with $E_d=0.289$ MeV. The neutron-induced reactions giving rise to the most prominent high-energy peaks are labeled. The few counts in channel numbers > 920 are due to reactions with ^{29}Si.

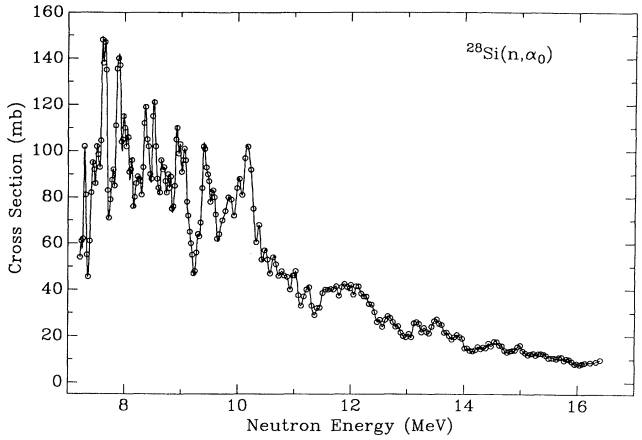

FIG. 2. Cross section for ^{28}Si$(n,\alpha_0)^{25}$Mg over the range measured in Ref. 16.

The signals from the four Si(Li) detectors were analyzed by 1024-channel analog-to-digital converters in conjunction with a CAMAC-data-aquisition system. The dead time (always < 5%) was monitored by counting the number of CAMAC strobes in a fast scaler and comparing that with the number of events processed by the CAMAC system. Detector resolution and energy calibration were checked with the prolific neutron-producing reactions ^{9}Be$(\alpha,n_0)^{12}$C and ^{3}H$(d,n)^4$He. The resolution in each detector was found to be ~125 keV when the kinematic spread of the incident neutrons was made negligible by moving the detector to a sufficient distance from the target. Background in the detectors due to sources other than neutron-producing reactions in the target was negligible in the high-energy region of interest. The ratio of active volumes of the detectors was checked with neutrons from ^{9}Be$(\alpha,n_0)^{12}$C in the following way. The yield in the ^{28}Si$(n,\alpha_0)^{25}$Mg peak was found for each of the detectors in identical geometry and with the same beam

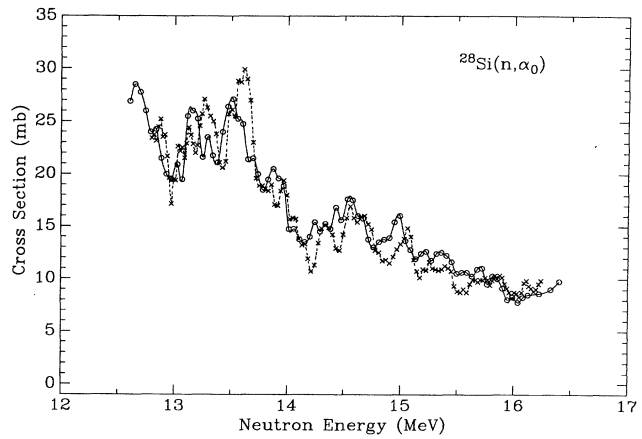

FIG. 3. Cross section for ^{28}Si$(n,\alpha_0)^{25}$Mg over the range of overlap of data from Ref. 16 (circles) and Ref. 17 (crosses).

energy. Tests with the 4π neutron detector indicated that the ^9Be target was uniform within 10%. The resulting active-volume ratios for three of the detectors were mutually consistent with the manufacturer's specifications, but one of the 75-mm^2 detectors had, by comparison, an active volume that was 50% below the specified value.

The number of counts Y in the $^{28}Si(n,\alpha_0)^{25}Mg$ peak is given by

$$Y = K_d \frac{d\sigma}{d\Omega} \sigma_{Si} \frac{Q}{Z} , \quad (1)$$

where $d\sigma/d\Omega$ is the differential cross section of interest in the target; σ_{Si} is the cross section (Fig. 2) for $^{28}Si(n,\alpha_0)^{25}Mg$ in the detector for the calculated neutron energy, Q is the integrated charge in μC, Z is the ^7Li charge state (1 or 2), and K_d is a constant for each detector proportional to the tritium areal density in the target and the active volume and acceptance solid angle of the detector. In practice, each detector subtends a finite solid angle, which means that the incident neutrons are spread in energy by kinematics. This effect was taken into account by averaging the $^{28}Si(n,\alpha_0)^{25}Mg$ cross section over the distribution of neutron energies in each detector, and was done in the analysis of all runs for $^3H(d,n)^4He$ and $^3H(^7Li,n_0)^9Be$.

For the measurement of the $^3H(^7Li,n_0)^9Be$ cross section, the four detectors were fixed in position at $\theta_{lab}=0°$, 45°, 90°, and 135°. Then, for each, the constant K_d in Eq. (1) was determined using the $^3H(d,n)^4He$ reaction, for which the differential cross section is known[19] to about 4%. For each detector configuration, runs were taken at $E_d=0.289$, 0.390, and 0.692 MeV. The deuteron energy was corrected for energy loss in the target, as described below for ^7Li. Counting statistics in each of the detectors in all of the $^3H(d,n)^4He$ calibration runs were always 4% or better.

In the neutron spectra at 135° from $^3H(d,n)^4He$, a broad peak at an energy slightly higher than the $^{28}Si(n,\alpha_0)^{25}Mg$ peak was evident (see Fig. 4), and is attributed to (d,n) reactions with dilute tritium distributed in the depth of the target. For $E_d<3.3$ MeV, the kinematics of the $^3H(d,n)^4He$ reaction at 135° are such that neutron energy *increases* as the incident deuteron energy *decreases*. Thus, the strong resonance in $^3H(d,n)^4He$, at $E_d=0.107$ MeV with width $\Gamma_{lab}\approx 0.120$ MeV, gives rise to the peak at higher energy. Using the $^3H(d,n)^4He$ cross section[19] and the stopping power for hydrogen in titanium,[20] it was calculated that roughly one tritium atom per 10^3 titanium atoms was required to give rise to a peak of the observed magnitude. This level of tritium density inside the target is consistent with a previous study of the distribution of tritium in Ti-T targets.[21] For other projectiles used with this target the effect is unimportant in the absence of strong low-energy resonances. The effect is most prominent in the run at $E_d=0.692$ MeV because the $^3H(d,n)^4He$ cross section is lower than in the other two runs. The 135° spectrum at this energy was not used for calculating K_d because of the uncertainty introduced by this effect. The remaining 135° spectra and all of the 90° spectra were used, with an $\sim$20% correction to the (n,α_0) yields due to this background. The spectra at 0° and 45° were not affected because, in these directions, the neutrons due to this effect are sufficiently lower in energy that they do not contribute background to the $^{28}Si(n,\alpha_0)^{25}Mg$ peak.

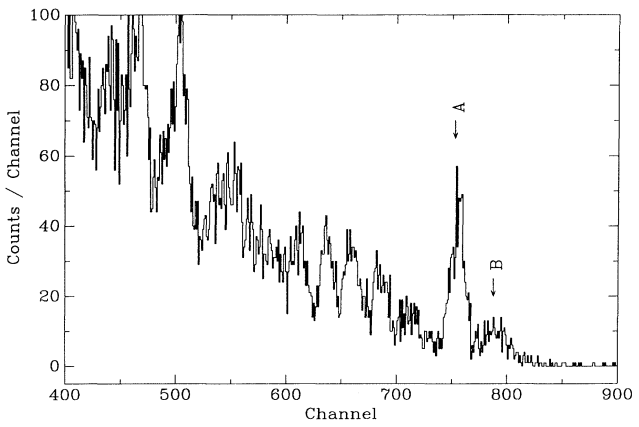

FIG. 4. Si(Li) pulse-height spectrum produced by neutrons from $^3H(d,n)$ at $\theta_{lab}=135°$ with $E_d=0.692$ MeV. The $^{28}Si(n,\alpha_0)^{25}Mg$ peaks arising from (d,n) reactions with surface tritium (A) and with tritium distributed in the depth of the target (B) are clearly visible.

For the purpose of calculating K_d, the average of the two previous measurements[16,17] of the $^{28}Si(n,\alpha_0)^{25}Mg$ cross section was used. The values of K_d obtained from the runs at 0° with the three different deuteron energies agreed within 6%, but the two runs at 135° differed by 25%. The values were averaged to arrive at a value of K_d for each detector. The calibrations obtained by this method agreed within 20% with calculations using the target tritium content, mean detector-target distance, and the manufacturers specifications for the active volume [when the active volume of one of the detectors was decreased by a factor of 2, as indicated by tests with $^9Be(\alpha,n_0)^{12}C$ described above].

The $^3H(^7Li,n_0)^9Be$ yield was measured for $0.50<E_{Li}<4.2$ MeV in steps varying from 100 to 400 keV. The runs were continued until better than 10% statistics were obtained in the $^{28}Si(n,\alpha_0)^{25}Mg$ peak in each detector. The $^3H(^7Li,n_0)^9Be$ differential cross sections were then calculated using Eq. (1) with σ_{Si} taken from Ref. 16. The ^7Li energy was corrected for energy loss in the target as described below. During the final runs with $E_{Li}>1.5$ MeV, a background extending beyond the $^{28}Si(n,\alpha_0)^{25}Mg$ peak was apparent, attributed to neutrons from $^2H(^7Li,n_0)$, which have higher energy than neutrons from $^3H(^7Li,n_0)^9Be$. This result was to be expected because a total of 22 mC of ^2H had been implanted in the target up to this time. This background was not present in earlier runs done in the same energy range on this target, prior to the (d,n) calibrations.

B. $^3H(^7Li,n_{tot})$

The neutron yield from $^3H(^7Li,n_{tot})$ was measured with the 4π neutron detector, which is described in more de-

tail elsewhere.[22] Briefly, the detector consists of a polyethylene-cube moderator 40 cm on each side with embedded thermal-neutron detectors. A 10-cm×10-cm open channel along the axis allows the insertion of a beam pipe. Twelve ^{3}He proportional counters are arranged in approximate cylindrical symmetry at a radius of ~12 cm from the beam axis. The whole detector system is movable on rails to allow access to the target, which was centered in the cube during measurements. A graphite moderator was used to fill the 10-cm×10-cm hole from 1 cm beyond the end of the beam pipe to the outside of the cube during all measurements. The relationship among the various experimental parameters is given by

$$Y=6.24\times10^{12}\sigma N_T\epsilon\frac{Q}{Z}\ , \tag{2}$$

where Y is the detector yield in counts, σ is the total cross section, N_T is the tritium areal density, ϵ is the detection efficiency, Q is the integrated charge in μC, and Z is the ^{7}Li charge state (1 or 2). The efficiency of the cube was calibrated with neutrons from a weak ^{252}Cf source whose strength is known to 3%. Previous tests with ^{7}Li(p,n) indicated that the efficiency of the detector is constant to better than 5% for neutrons of energies up to 2 MeV. The comparison of ^{3}H$(p,n)^3$He and ^{3}H$(d,n)^4$He yields indicated that the detection efficiency for 15-MeV neutrons is only 30% of that for ~1-MeV neutrons. The energy distribution of neutrons from ^{3}H$(^7$Li$,n_{\rm tot})$ is largely unknown and the detector efficiency between 2 and 15 MeV has not been calibrated, so only the following crude correction for the nonconstant efficiency is possible. Since most of the reaction channels contributing to ^{3}H$(^7$Li$,n_{\rm tot})$ produce two neutrons per reaction, we assume that half of the neutrons were emitted with an energy of 8 MeV [which are detected with ~60% of the efficiency for ^{3}H$(p,n)^4$He neutrons], and that the other half were emitted with an energy of 1 MeV [which are detected with the same efficiency as for ^{3}H$(p,n)^3$He neutrons]. The result of this assumption is that the efficiency for ^{3}H$(^7$Li$,n_{\rm tot})$ neutrons is 80% of the efficiency for ^{3}H$(p,n)^3$He neutrons. The total cross sections reported here used this estimated efficiency, and are assigned an overall normalization error of 15% due to efficiency uncertainty.

The ^{3}H$(^7$Li$,n_{\rm tot})$ yield was measured for $0.33<E_{\rm c.m.}<5.0$ MeV, using a thin zirconium-tritide (Zr-T) target on a platinum backing supplied by Amersham Corporation. No target cooling was applied, so beam currents were kept <50 nA. A blank target, which consisted of zirconium on a platinum backing with no tritium, was also available, and could be easily exchanged with the tritium target to monitor background without breaking vacuum. With this tritium target, only 2 of the 12 ^{3}He proportional counters were used in order to reduce the count rate. The efficiency for ^{252}Cf neutrons in this configuration was found to be 3.77±0.15 %. The tritium areal density, $N_T=(1.98\pm0.20)\times10^{16}$ atoms/cm^2, was found by measuring the ^{3}H$(p,n)^3$He yield in the 4π neutron detector at $E_p=1.300$ and 1.500 MeV, and averaging the two resulting values of N_T. The cross section for ^{3}H$(p,n)^3$He is known[19] to a precision of 7%. Target uniformity was tested with ^{3}H$(p,n)^3$He by measuring the yield from different locations on the target, and found to be constant within 5%. For $E_{\rm Li}>5.00$ MeV, a background rising sharply with energy was observed on the blank target. A similar rise was also seen in the yield from the tritium target, prompting us not to use data for $E_{\rm Li}>5.00$ MeV. No correction was made for ^{7}Li energy loss in the target, since the target was quite thin ($\lesssim$8 keV).

The ^{3}H$(^7$Li$,n_{\rm tot})$ yield was measured for $0.22<E_{\rm c.m.}<0.99$ MeV, using the thicker Ti-T target, described in Sec. I A. Again, using ^{3}H$(p,n)^3$He yields, at $E_p=1.300$ and 1.500 MeV, with two ^{3}He counters active, we found $N_T=(1.47\pm0.15)\times10^{17}$ atoms/cm^2. This target was also found to be uniform within 5%. With 11 ^{3}He counters active (the twelfth had developed noise problems), the efficiency for ^{252}Cf neutrons was found to be 19.1±1.0 %. Measurements at still lower energies were not possible due to the inability of the accelerator to regulate the required low terminal voltages. The yield was converted to a cross section using Eq. (2), after applying corrections to determine the effective ^{7}Li energies in the thicker Ti-T target as described in the following section.

C. Correction for ^{7}Li energy loss in target

Beam energies for the runs on the thicker Ti-T target required correction for ^{7}Li energy loss in the target. In order to determine the tritium distribution in depth in the target, γ rays from ^{3}H(α,γ_0) at $E_\alpha=998.1\pm1.0$ keV were observed at 0° with a 160-cm^3 high-purity germanium detector. The γ-ray energy calibration was provided by well-known background lines. With ^{3}H(α,γ_0) kinematics, the centroid and width of the ^{3}H(α,γ_0) photopeak determine, respectively, the mean energy and energy spread of the α particles reacting with tritium. The contribution to the width of the photopeak from the resolution of the detector was subtracted in quadrature from the measured width. The detector was sufficiently far away from the target that the Doppler spread was negligible. The α-particle energy for the centroid was found to be shifted by 34.2±1.0 keV. The rms energy deviation of the α particles was found to be 10.5 keV; the width at half maximum was 28 keV.

These values were then converted to energy shifts and spreads for ^{7}Li using the stopping powers for α particles and ^{7}Li in titanium.[20] The shift in ^{7}Li mean energy was the most important effect, varying between 49.3±7.4 and 57.0±8.6 keV for the energies covered in this experiment. This correction was applied to all data taken with the Ti-T target. The spread of ^{7}Li energy in the target had an important effect for the ^{3}H$(^7$Li$,n_{\rm tot})$ data only at low energy. Here, since the energy dependence of the cross section is dominated by the Coulomb barrier, it is simplest to consider the astrophysical S factor defined by

$$\sigma(E)=\frac{S(E)}{E}\exp(-\sqrt{E_G/E}\ )\ , \tag{3}$$

where E is the center-of-mass energy and E_G is the

Gamow energy (18.584 MeV). In the presence of a distribution of reaction energies, Eq. (2) is replaced by

$$Y=6.24\times10^{12}\sigma(E)N_T\epsilon\frac{Q}{Z}\left[1+F(E)\frac{\Delta E^2}{E^2}\right] \quad (4)$$

with

$$F(E)=\frac{E_G}{8E}-\tfrac{7}{8}\sqrt{E_G/E}+1\ ,$$

where E is the corrected center-of-mass energy and ΔE is the rms energy spread in center of mass. This formula assumes a constant $S(E)$ and includes effects up to the second moment of the distribution. Since this correction is small (20% for the lowest point, but dropping to 3% at $E_{c.m.}=0.100$ MeV), the approximation of constant $S(E)$ should not appreciably increase the uncertainty in $\sigma(E)$.

III. RESULTS

A. $^3H(^7Li,n_0)^9Be$

A sample Si(Li) pulse-height spectrum produced by neutrons from $^3H+^7Li$ is shown in Fig. 5. The laboratory cross sections $d\sigma/d\Omega$ were extracted according to the procedure described in Sec. II A. The data were assigned an uncertainty of 15%, primarily because of the uncertainty and fluctuations of the $^{28}Si(n,\alpha_0)^{25}Mg$ cross section. The $^3H(^7Li,n_0)^9Be$ cross sections at the four angles were converted to center of mass and fitted with a (fully determined) set of Legendre polynomials:

$$\left[\frac{d\sigma}{d\Omega}\right]_{c.m.}=\sum_{l=0}^{3}A_lP_l(\cos\theta_{c.m.})\ . \quad (5)$$

The total cross section is then given by $\sigma=4\pi A_0$. The center-of-mass cross sections are consistent with isotropy at low energies ($E_{c.m.}<0.3$ MeV), and at higher energies become peaked at backward angles (see Fig. 6). The total cross section is presented in Fig. 7, and the $S(E)$ [Eq. (3)] is plotted in Fig. 8. The energy dependence is essentially the same as that found for $^3H(^7Li,n_{tot})$, as shown in Fig. 8 by the solid line, which is the fit to our $^3H(^7Li,n_{tot})$ data (described below) normalized by a factor of 0.0403.

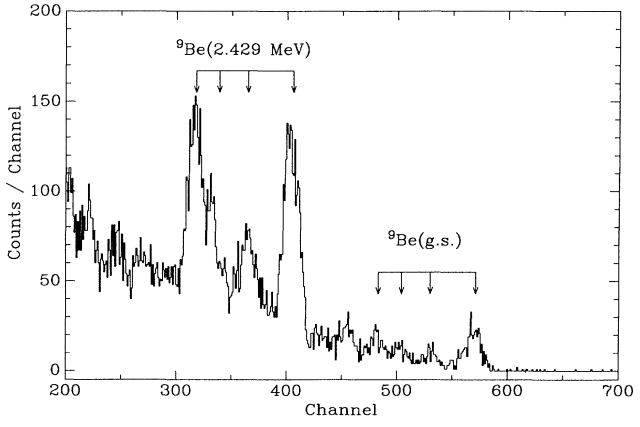

FIG. 5. Si(Li) pulse-height spectrum produced by neutrons from $^3H+^7Li$ at $\theta_{lab}=0°$ with $E_{^7Li}=0.648$ MeV. The multiple peaks due to $^3H(^7Li,n_0)^9Be$ and $^3H(^7Li,n_2)^9Be(2.429)$ are clearly resolved, as indicated, the right-most peak in each group being due to $^{28}Si(n,\alpha_0)^{25}Mg$.

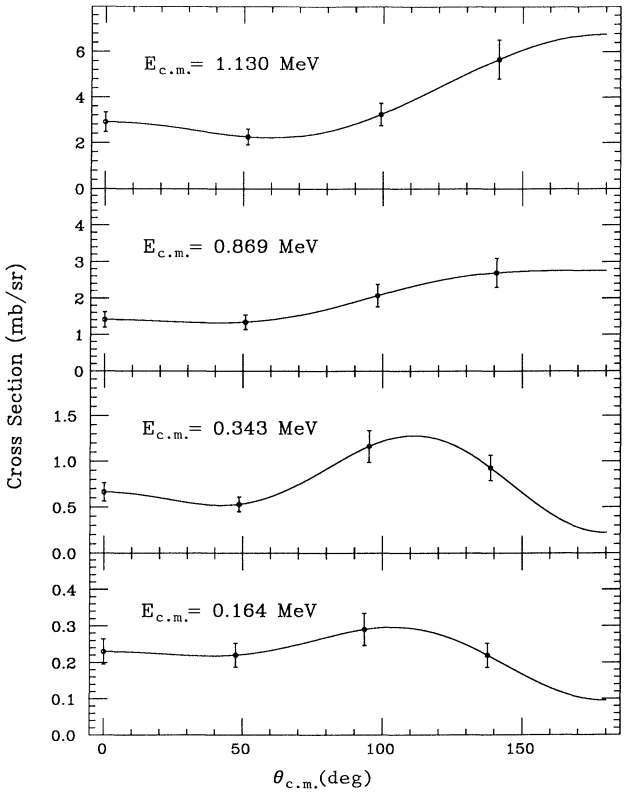

FIG. 6. Examples of the measured $^3H(^7Li,n_0)^9Be$ center-of-mass differential cross sections. The curves are fully determined fits with the lowest four Legendre polynomials, used for convenience in extracting the total cross sections.

For several energies below $E_{c.m.}=0.5$ MeV, the decreased kinematic spread of the neutrons improved the resolution of the spectra sufficiently to resolve the yield of neutrons from $^3H(^7Li,n_2)^9Be(2.429)$. The neutron energies at $\theta_{lab}=135°$ were below the range where the $^{28}Si(n,\alpha_0)^{25}Mg$ cross section has been measured, so these data were not analyzed. The remaining cross sections were converted to center of mass and integrated numerically with a $\sin\theta$ weighting to obtain total cross sections, shown as triangles in Fig. 7.

Although the $^3H(^7Li,n_0)^9Be$ reaction has not been previously studied, the inverse reaction $^9Be(n,^3H)$ has been (see Zadro *et al.*[23] for a review). A recent study[24] of the total tritium-production cross section for $^9Be(n,^3H_{0+1})$, which (for $E_n<14.34$ MeV) proceeds through the ^7Li ground state and first excited state, found $\sigma=16.1\pm1.0$ mb at $E_n=13.30\pm0.03$ MeV (these numbers are interpolations of their data, but their data points are closely spaced with monotonic energy dependence). Their data were taken with a spread of neutron energies with a full

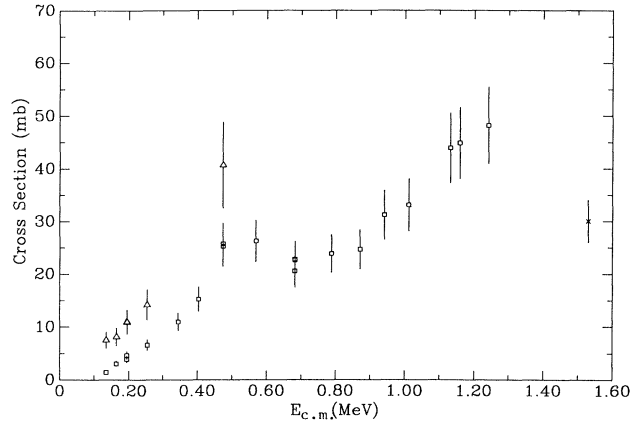

FIG. 7. The measured ^{3}H(^{7}Li,n_0)^{9}Be total cross section (squares). The ^{3}H(^{7}Li,n_2)^{9}Be(2.429) cross section is also shown (triangles) for energies at which the corresponding α_0 peaks were clearly resolved (the peak for $E_{c.m.}=0.47$ MeV was resolved because the detectors were farther away from the target than for the other runs). The datum (cross) at $E_{c.m.}=1.5$ MeV is the value derived from the inverse-reaction measurements in Refs. 24 and 25.

width of 150 keV. A study[25] of the ^{9}Be(n,^{3}H$_1$) cross section (i.e., to the first excited state of ^{7}Li) found $\sigma=7.3\pm0.7$ mb at $E_n=13.3\pm0.1$ MeV, with a neutron-energy spread estimated to be 250 keV. The combination of these results yields $\sigma=8.8\pm1.2$ mb at $E_n=13.3\pm0.1$ MeV for the ground-state to ground-state channel. The principle of detailed balance then gives $\sigma=30\pm4$ mb at $E_{c.m.}=1.53\pm0.09$ MeV for ^{3}H(^{7}Li,n_0)^{9}Be. This cross section is similar in magnitude to that obtained in our measurement, although the energy is beyond the range covered by our data (see Fig. 7). At higher energies, the existing data on the inverse reaction indicate that the cross section remains approximately constant ($\sigma\approx30$ mb) up to $E_{c.m.}=3$ MeV.

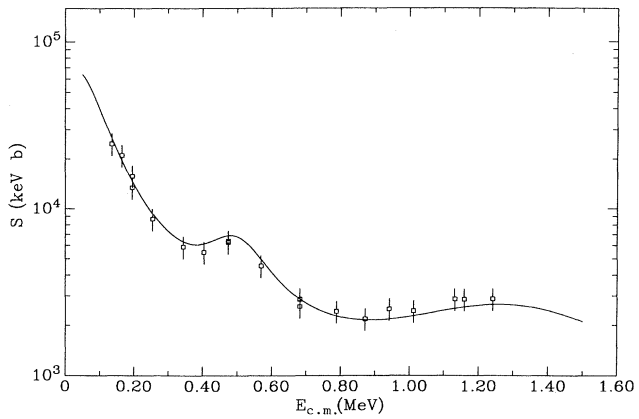

FIG. 8. The S factor for ^{3}H(^{7}Li,n_0)^{9}Be. The curve is the same as in Fig. 10, scaled by a constant factor 0.0403.

B. ^{3}H(^{7}Li,n_{tot})

The cross section and $S(E)$ for ^{3}H(^{7}Li,n_{tot}) are shown in Figs. 9 and 10, respectively. The error bars reflect uncertainties in counting statistics, target uniformity, and the correction for ^{7}Li energy loss in the Ti-T target; the uncertainty in normalization is not included. A sum of Breit-Wigner functions of the form

$$S(E)=\sum_{i=1}^{3}\frac{H_i(\Gamma_i/2)^2}{(E-E_i)^2+(\Gamma_i/2)^2} \tag{6}$$

was fitted to $S(E)$, and the resulting parameters are presented in Table I. The errors quoted for the fitting parameters reflect the error associated with the fit, and do not include errors in the normalization of the data or the assumed form of $S(E)$. In the region where the data sets from the two targets overlapped, data from the Ti-T target were used. Three Breit-Wigner functions were sufficient to fit the data (see Fig. 10), although there is some evidence for additional structure in the vicinity of $E_{c.m.}=0.40$ MeV. The fit indicates resonances at $E_{c.m.}=0.028\pm0.005$, 0.493 ± 0.004, and 1.289 ± 0.012 MeV with widths $\Gamma_{c.m.}=170\pm4$, 211 ± 15, and 862 ± 51 keV, respectively. The inclusion of an additional resonance at $E_{c.m.}=0.40$ MeV improved the quality of fit (reduction of χ^2 by a factor of 2), and shifted the position of the 0.493-MeV resonance up in energy by 0.022 MeV; however, in the interest of simplicity, three resonance terms were deemed sufficient. The resonances parameters found here are to be compared with previous studies by Val'mer *et al.*,[9] who found broad resonances at $E_{c.m.}=0.536$ and 1.215 MeV, and Serov and Guzhovskii,[10] who found a broad resonance at $E_{c.m.}$

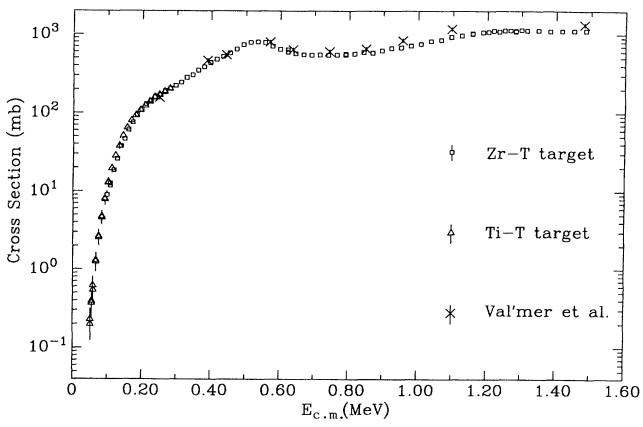

FIG. 9. The total cross section for ^{3}H(^{7}Li,n_{tot}) found using the Ti-T and Zr-T targets. The cross section found by Val'mer *et al.* (Ref. 10) is shown for comparison.

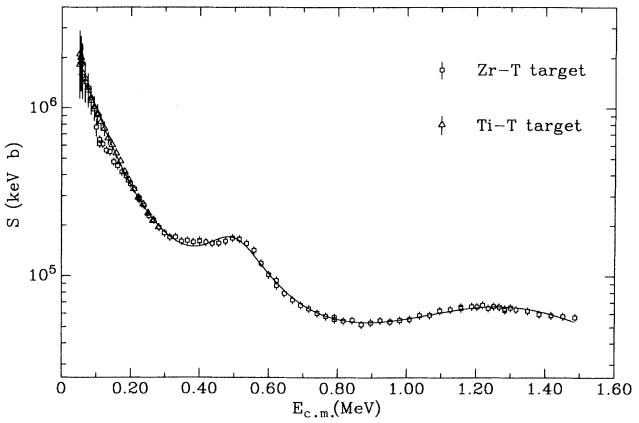

FIG. 10. The S factor for $^3H(^7Li,n_{tot})$ obtained using the Ti-T and Zr-T targets. The fit by Eq. (6) is also shown for the parameters in Table I.

$=0.497\pm0.014$ MeV. The S factor rises steeply with decreasing energy, in agreement with the previous work, and leads through Eq. (6) to the assignment of the resonance at $E_{c.m.}=0.028$ MeV. For $E_{c.m.}<0.8$ MeV, the energy dependence and normalization of the total cross section agree well with that found by the Val'mer *et al.*, but for $E_{c.m.}>0.9$ MeV our result is lower by 20%.

C. Reaction rates

The thermonuclear reaction rate $N_A\langle\sigma v\rangle$ for $^3H(^7Li,n_0)^9Be$ is given by[26]

$$N_A\langle\sigma v\rangle=2.98\times10^{10}T_9^{-2/3}\exp\left[-\frac{11.333}{T_9^{1/3}}\right]\left[1-0.122T_9^{2/3}+\frac{1.32}{T_9^{4/3}-0.127T_9^{2/3}+0.0742}\right](\mathrm{cm^3\,s^{-1}\,mol^{-1}})\,. \quad (8)$$

The reaction rate for $^3H(^7Li,n_{tot})$ (Fig. 11, curve D) was calculated by the same procedure, using Eq. (6) and the parameters in Table I for $S(E)$ for $E_{c.m.}<1.5$ MeV and $\sigma=744$ mb for higher energies. This procedure yields a rate equal to 24.8 times Eq. (8). The contribution to this rate from $E_{c.m.}<0.051$ MeV was 10% at $T_9=0.1$, while the contribution from $E_{c.m.}>1.5$ MeV was 50% at $T_9=10$. It should be noted that most of the reaction channels contributing to $^3H(^7Li,n_{tot})$ produce *two* neutrons per reaction, so this is strictly only the rate for producing neutrons.

IV. CONCLUSION

The measured reaction rate for $^3H(^7Li,n_0)^9Be$, curve A in Fig. 11, is generally lower than that (curve B) assumed by Malaney and Fowler,[7] but exceeds their assumed rate for $T_9<0.5$. The measured rate is considerably lower than that (curve C) assumed by Boyd and Kajino,[3] and also lower than the rate (not shown in Fig. 11, but similar to curve C) inferred by Rath *et al.*[27] from their measurements of the $^7Li(^3He,p)^9Be$ reaction. The reaction rates

TABLE I. Parameters returned by fit of Eq. (6) to $S(E_{c.m.})$ for $^3H(^7Li,n_{tot})$.

E_i (MeV)	Γ_i (MeV)	H_i (keV b)
0.028±0.005	0.170±0.004	$(1.67\pm0.09)\times10^6$
0.493±0.004	0.211±0.012	$(1.03\pm0.04)\times10^5$
1.289±0.012	0.862±0.048	$(5.65\pm0.09)\times10^4$

$$N_A\langle\sigma v\rangle=\left[\frac{8}{\mu\pi}\right]^{1/2}\frac{N_A}{(kT)^{3/2}}\times\int_0^\infty S(E)\exp\left[-\frac{E}{kT}-\sqrt{E_G/E}\right]dE\,, \quad (7)$$

where μ is the reduced mass in the entrance channel, k is Boltzmann's constant, T is the temperature, and E is the energy in the center of mass. The integration was performed numerically, using Eq. (6) and the parameters in Table I normalized by 0.0403 for $S(E)$ (see Fig. 8 for quality of fit) for $E_{c.m.}<1.5$ MeV, and a constant $\sigma=30$ mb for higher energies (as indicated by the inverse reaction). In Fig. 11, curve A shows the results for the reaction rate vs T_9, the temperature in units of 10^9 K. The contribution to the rate from $E_{c.m.}<0.134$ MeV (i.e., below our data range) was 30% at $T_9=0.4$, while the contribution from $E_{c.m.}>1.24$ MeV (the highest energy measured) was 60% at $T_9=10$. An analytic form for the reaction rate, agreeing to ±6% for $T_9<10$ with the rate determined above, is given by

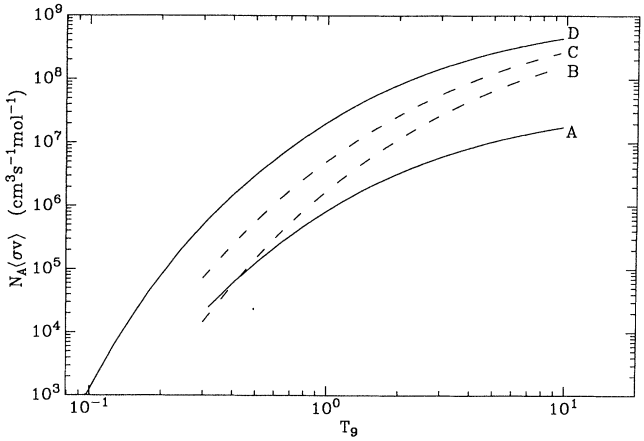

FIG. 11. The thermonuclear reaction rate $N_A\langle\sigma v\rangle$ for $^3H(^7Li,n_0)^9Be$ (solid curve A) obtained from the experimental data. The rates for $^3H(^7Li,n_0)^9Be$ assumed by Malaney and Fowler[7] (dashed curve B) and Boyd and Kajino[3] (dashed curve C) are shown for comparison. The rate for $^3H(^7Li,n_{tot})$ (solid curve D) found from our experimental data is also shown.

found here provide an experimental basis for predictions of primordial ^{9}Be nucleosynthesis, which, coupled with the recent increase in observational sensitivity,[5] may allow new constraints to be placed on primordial nucleosynthesis. It should be pointed out, however, that questions about the modeling of primordial nucleosynthesis still exist.[8]

ACKNOWLEDGMENTS

The authors thank R. E. Azuma and the University of Toronto for providing the titanium-tritide target used in these experiments. This work was supported by the National Science Foundation Grant No. PHY88-17296.

[1]E. Witten, Phys. Rev. D **30**, 272 (1984).
[2]H. Kurki-Suonio and R. A. Matzner, Phys. Rev. D **39**, 1046 (1990).
[3]R. N. Boyd and T. Kajino, Astrophys. J. Lett. **336**, L55 (1989).
[4]R. Rebolo, P. Molaro, C. Abia, and J. E. Beckman, Astron. Astrophys. **193**, 193 (1988).
[5]S. G. Ryan, M. S. Bessell, R. S. Sutherland, and J. E. Norris, Astrophys. J. Lett. **348**, L57 (1990).
[6]T. Kajino and R. N. Boyd, Astrophys. J. **359**, 267 (1990).
[7]R. A. Malaney and W. A. Fowler, Astrophys. J. Lett. **345**, L5 (1989).
[8]N. Terasawa and K. Sato, Astrophys. J. Lett. **362**, L47 (1990).
[9]A. K. Val'mer, P. I. Vatset, L. Ya. Kolesnikov, S. G. Tonapetyan, K. K. Chernyavskii, and A. I. Shpetnyi, At. Energ. **10**, 577 (1961) [Sov. J. At. Energy **10**, 574 (1961)].
[10]V. I. Serov and B. Ya. Guzhovskii, At. Energ. **12**, 11 (1962) [Sov. J. At. Energy **12**, 1 (1962)].
[11]R. W. Crews, Phys. Rev. **82**, 100 (1951).
[12]R. Seltz and D. Magnac-Valette, C. R. Acad. Sci. **251**, 2006 (1960).
[13]T. R. Wang, R. B. Vogelaar, and R. W. Kavanagh, Phys. Rev. C **43**, 883 (1991).
[14]J. W. Maas, A. J. C. D. Holvast, A. Baghus, H. J. M. Aarts, and P. M. Endt, Nucl. Phys. **A301**, 237 (1978).
[15]S. K. Allison, J. Cuevas, and M. Garcia-Munoz, Phys. Rev. **120**, 1266 (1960).
[16]R. G. Miller and R. W. Kavanagh, Nucl. Instrum. Methods **48**, 13 (1967).
[17]D. W. Mingay, J. P. F. Sellschop, and P. M. Johnson, Nucl. Instrum. Methods **94**, 497 (1971).
[18]C. M. Lederer and V. S. Shirley, *Table of Isotopes*, 7th ed. (Wiley, New York, 1978).
[19]H. Liskien and A. Paulsen, Nucl. Data Tables **11**, 569 (1973).
[20]J. F. Ziegler, *The Stopping and Ranges of Ions in Matter* (Pergamon, New York, 1977), Vols. 3–5.
[21]E. M. Gunnersen and G. James, Nucl. Instrum. Methods **8**, 173 (1960).
[22]S. E. Kellogg and R. W. Kavanagh (unpublished).
[23]M. Zadro, S. Blagus, D. Miljanić, and D. Rendić, Nucl. Sci. Eng. **95**, 79 (1987).
[24]H. Liskien, R. Widera, R. Wölfle, and S. M. Qaim, Nucl. Sci. Eng. **98**, 266 (1988).
[25]F. S. Dietrich, L. F. Hansen, and R. P. Koopman, Nucl. Sci. Eng. **61**, 267 (1976).
[26]C. E. Rolfs and W. S. Rodney, *Cauldrons in the Cosmos* (University of Chicago Press, Chicago, 1988), p. 158.
[27]D. P. Rath, R. N. Boyd, H. J. Hausman, M. S. Islam, and G. W. Kolnicki, Nucl. Phys. **A515**, 338 (1990).